Role of Atrial Tissue Substrate and Electrical Activation Pattern in Fractionation of Atrial Electrograms: a Computational Study

Marta Varela and Oleg V. Aslanidi

***Abstract*— Complex fractionated atrial electrograms (CFAEs) are often used as a clinical marker for re-entrant drivers of atrial fibrillation. However, outcomes of clinical ablation procedures based on CFAEs are controversial and the mechanistic links between fractionation, re-entrant activity and the characteristics of the atrial substrate are not completely understood. We explore such links by simulating electrograms arising from both normal and re-entrant electrical activity in atrial tissue models. 2D and 3D tissue geometries with a range of conditions for intracellular coupling and myofiber orientation fields were studied. Electrograms were fractionated in the presence of complex atrial fiber fields and in 3D irregular geometries, due to far-field excitations. The complexity of the local electrical activity was not a strong determinant of the degree of fractionation. These results suggest that electrogram fractionation is more strongly linked to atrial substrate characteristics (including tissue geometry, fiber orientation and degree of intercelullar coupling) than to the electrical activation pattern sustaining atrial fibrillation.**

I. INTRODUCTION

Atrial fibrillation (AF) is a disturbance in the rhythm of the heart, characterized by rapid and disorganized activation of the atria. Despite its major health and socio-economic impact, the mechanisms underlying AF and its optimal treatment course are still incompletely understood. Catheter ablation procedures for persistent AF are commonly performed, but suffer from low success rates and high AF recurrence [1]. Empirical markers of re-entrant drivers of AF, such as complex fractionated atrial electrograms (CFAEs) detected using local catheter mapping [2], have been suggested to improve the outcome of ablation procedures.

The term complex fractionated atrial electrograms is commonly used to describe atrial electrograms that show several tightly-clustered, low-amplitude and high-frequency deflections. Although CFAEs are highly non-specific and can be observed in healthy subjects in sinus rhythm [3], they are often used as a marker for fibrillatory electrical activity in AF [4]. However, results of clinical ablation procedures based on CFAE markers alone or in combination with pulmonary vein isolation are variable [5].

These disparate results may be explained by the fact that it is unclear what CFAE morphologies represent. Modelling and experimental studies have shown that CFAEs can have various origins, including: signal processing artefacts and contamination with ventricular signals [6]; activation in remote [6], anisotropic [7] or poorly coupled regions [8] and abnormal electrical activity, such as conduction block, wavefront collisions or re-entrant circuits [4]. However, the understanding of the mechanistic significance of CFAE morphologies and underlying factors is incomplete.

Computational modelling provides a quantitative framework for integrating multiple underlying factors of AF and dissecting the mechanisms behind CFAEs. Previous modelling studies of CFAEs have mostly been performed in 2D and have mainly focused on the effect of fibrosis on CFAEs [8], [9]. One study used an MRI-based atrial geometry, but no atrial thickness was included and fiber orientations were manually drawn, failing to detect any fractionated electrograms [10].

In this paper, we explore the relative contribution of atrial tissue substrate and electrical activity associated with AF on atrial electrograms. The impact of fiber orientation, degree of intercellular coupling and anisotropy and the type of activation (regular wavefront, re-entry) on electrogram fractionation is qualitatively assessed. For this purpose, we employ 2D rectangular models and also 3D models based on dog atria reconstruction from high-resolution micro-computed tomography.

II. METHODS

A. Atrial Simulations

The monodomain reaction-diffusion equation

$$\frac{\partial V_m}{\partial t} = \nabla . D \nabla V_m - \frac{I_{ion}}{C_m} \tag{1}$$

(where V_m is the transmembrane potential, t is time, C_m is the membrane capacitance, I_{ion} is the transmembrane ionic current per unit area and D is the electrical diffusion tensor) was solved using a finite differences method in a regular Cartesian grid, with a time step of 2.5 μs, a spatial step of 0.3 mm and Neumann boundary conditions. The degree of intercellular coupling was altered by varying the longitudinal diffusion coefficient ($D_{||}$) and the anisotropy ratio (AR) between longitudinal and transverse diffusion coefficients. The ionic models used are based on the Ramirez-Nattel-Courtemanche model [11], modified according to the latest electrophysiological data from the canine right atrium (RA) [12] and AF-induced ionic channel remodeling [13].

Simulations were run in two different geometries: a 88.2x88.2 mm^2 rectangle and a 23.7x21.0x23.7 mm^3 segment of the RA, with a geometry obtained from the segmentation of a high-resolution canine micro-computed tomography scan [14] and detailed orientation of myofibers

Research supported by the British Heart Foundation (PG/10/69/28524) and the King's College London BHF Centre of Research Excellence. Both authors are with the Department of Biomedical Engineering, Division of Imaging Sciences, St Thomas' Hospital Campus, King's College London, London, UK (e-mail: marta.varela@kcl.ac.uk; oleg.aslanidi@kcl.ac.uk; phone: +44 (0) 20 7188 8299).

978-1-4244-7929-0/14/$26.00

computed using structure tensor analysis [15]. The fiber orientation for the rectangle was either at 45° with the x and y axes in all voxels or was mapped from a flattened portion of the RA. Integration of canine tissue architecture and electrophysiology into 3D biophysical models has been described in detail previously [16], [17].

In a first study, one of the corners of the geometry was paced every 300 ms to simulate sinus rhythm pacing in the dog. In a second study, re-entry was initiated using a cross-field protocol at several values of $D_{||}$ and AR to simulate re-entry conditions with different wavelengths and number of wavefronts.

B. Electrogram Computation

Electric potentials outside the heart were computed using the formalism first used by Spach for anisotropic tissue [7]:

$$\phi_e = K \iiint \frac{\nabla . D \nabla V_m}{\sqrt{(x-x_e)^2 + (y-y_e)^2 + (z-z_e)^2}} \, dx \, dy \, dz \tag{2}$$

where ϕ_e is the electric potential measured in one electrode (in arbitrary units) and (x_e, y_e, z_e) are the positions of the electrode in the (x, y, z) Cartesian grid. K is a scalar constant that determines the units in which ϕ_e is measured and which was arbitrarily set to 1 in our study. Electrodes were placed 0.6 mm away from the surface along the normal vector, with a mean inter-electrode spacing of 2.4 mm. ϕ_e was computed every 1 ms. These values were chosen to match experimental parameters [18].

To assess how accurately the timings of local activation could be detected using electrograms, local activation time maps were computed by finding the times at which $\frac{\partial \phi_e}{\partial t}$ was most negative, as in experimental studies [18]. These were compared with true voxel activation times ($\frac{\partial V_m}{\partial t} > 10$ V/s) in the computational model.

III. RESULTS

A. Regular Wavefronts

In the rectangular 2D tissue with a uniform fiber orientation, all electrograms showed a single biphasic peak whose amplitude was proportional to a constant D in the isotropic case, as expected from (2) (Figs 1 a, b). The activation time estimated from the electrogram matched the tissue activation in all situations and electrodes (Fig 1 a, b).

For simulations with fiber orientations taken from the RA (Fig 1c), electrograms from all electrodes showed several high-frequency, low-amplitude peaks concomitant with the local activation peak, which led to incorrect estimates of arrival time in some electrodes.

In the RA segment, all electrograms showed several high-frequency low-amplitude peaks caused by far-field signals, particularly from tissue regions with irregular geometrical features, such as the pectinate muscles (PMs) (Fig 2). These were present in both isotropic (Fig 2a) and anisotropic (Fig 2b) simulations, indicating the importance of tissue geometry in electrogram morphology. As the far-field activity overlapped with the local activation peak, erroneous estimates of local activation time were seen in several electrodes (Fig 2).

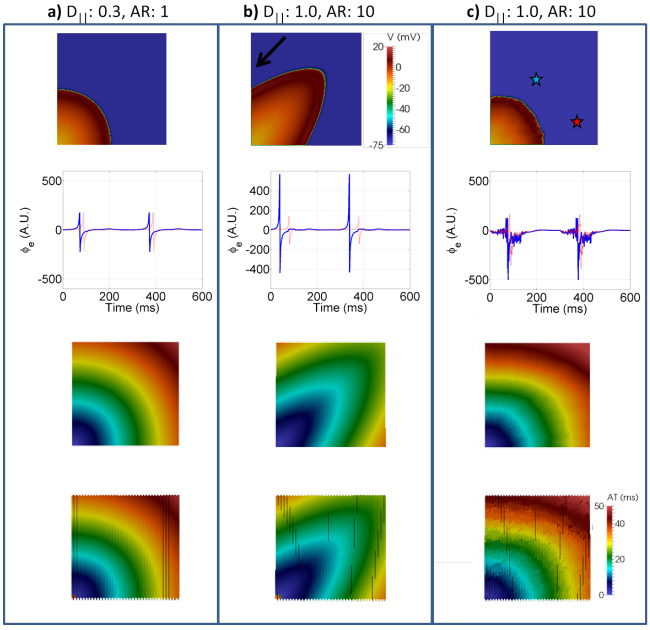

Fig. 1. Regular wavefronts in the rectangular geometry. Electrical potential maps at t = 50 ms (top row, scale shown in panel b), two representative electrode tracings (second row), true activation time maps (third row) and activation time maps computed using electrograms (bottom row). (Some interpolation artefacts can be seen in the bottom row.) **a)** isotropic fiber field, **b)** uniform diagonal fiber field (direction given by black arrow in top left corner); **c)** non-uniform fiber field taken from a portion of the right atrium. The longitudinal diffusion coefficient ($D_{||}$, in mm^2/ms) and diffusion anisotropy ratio (AR) for each panel are shown above it. The in-plane position of the electrodes whose traces are displayed is marked by two matching color stars in panel c).

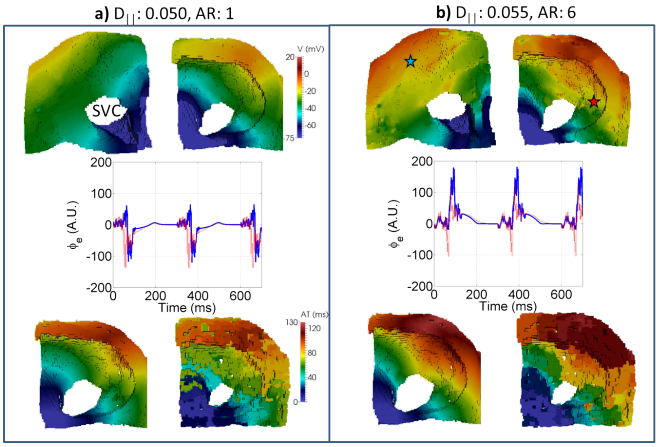

Fig. 2. Regular pacing in a segment of the right atrium. **Top row:** electrical potential maps at t =140 ms (scale shown in panel b), showing epicardial (left) and endocardial (right) views. The smaller orifice corresponds to the superior vena cava (SVC) and the larger one to the right atrio-ventricular ring. The pectinate muscle network (PMs) can be seen to the right of the SVC in the endocardial surface. **Middle row:** two representative electrode tracings. **Third row:** endocardial view of true activation time maps (left) and activation time maps computed using the electrograms (right). The longitudinal diffusion coefficient ($D_{||}$, in mm^2/ms) and diffusion anisotropy ratio (AR) for each panel are shown above it. The in-plane position of the electrodes whose traces are displayed is marked by two matching color stars in panel b).

B. Re-entry

The macroscopic complexity of electrical patterns shown in Figs. 3 a-c appears similar, with 3-4 rotors meandering in the tissue in all cases, with frequent wavelet collisions and break-ups. However, the resulting electrogram appearance was markedly different. Electrograms showed no fractionation for the 2D geometry with a uniform fiber orientation, in both isotropic (Fig 3a) and highly anisotropic tissue (3c), but the activation peaks displayed a marked asymmetry not seen in the single pacing case (compare with Fig 1 a, b). Electrograms showed a high degree of fractionation only in the case of a complex fiber arrangement (Fig 3b). This gives evidence to the crucial role of tissue substrate in electrogram morphology: both large tissue geometry features (Fig 2) and fiber micro-architecture (Fig 3b) have a greater effect of the electrogram fractionation than the complexity of the electrical pattern.

Filtering the fractionated signal in Fig 3b with a 12th-order Butterworth bandpass filter (30-250 Hz) as is commonly done experimentally [19] did not improve the separation of the activation peaks from the remaining signal.

In the RA segment with various degrees of anisotropy and electrical pattern complexity, unipolar electrograms displayed a similar morphology, with the signal always characterized by high-frequency low amplitude peaks. These were present when the tissue sustained several re-entrant wavefronts (Fig 4a), when there was a single wavefront anchored to the superior vena cava (Fig 4b) and in isotropic conditions (Fig. 4c). As in the rectangular geometry, signal filtering did not allow the local activation peaks to be separated from the remaining signal.

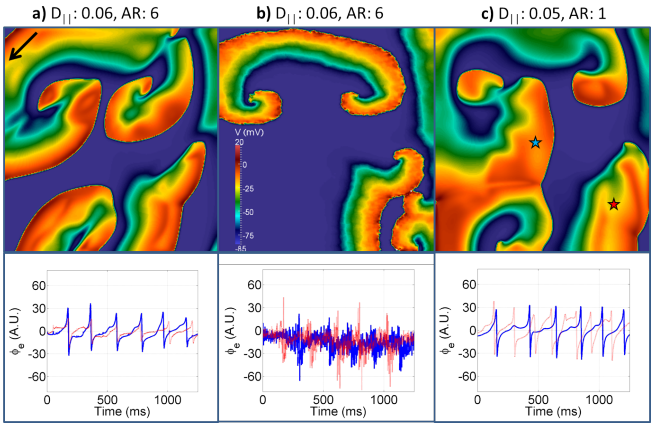

Fig. 3. Re-entry in the rectangular geometry. Electrical potential maps at t = 175 ms (top row, scale shown in panel b) and two representative electrode tracings (middle row) for: **a)** uniform diagonal fiber field (direction given by black arrow in top left corner); **b)** non-uniform fiber field taken from a portion of the right atrium; **c)** isotropic fiber field. The longitudinal diffusion coefficient ($D_{||}$, in mm^2/ms) and diffusion anisotropy ratio (AR) for each panel are shown above it. The in-plane position of the electrodes whose traces are displayed is marked by two matching-color stars in panel c).

IV. CONCLUSION

We applied computational models of atrial electrophysiology to investigate several conditions in which low-amplitude, high-frequency peaks, qualitatively similar to CFAEs linked with electrical excitations in AF [2] can arise in atrial electrograms. CFAE morphologies were seen in rectangular tissue in the presence of a complex fiber orientation field, due to simultaneous activation of tissue in several different directions, and also in both isotropic and anisotropic 3D tissues, suggesting that far-field excitations form the main contribution to this effect in 3D atrial tissue.

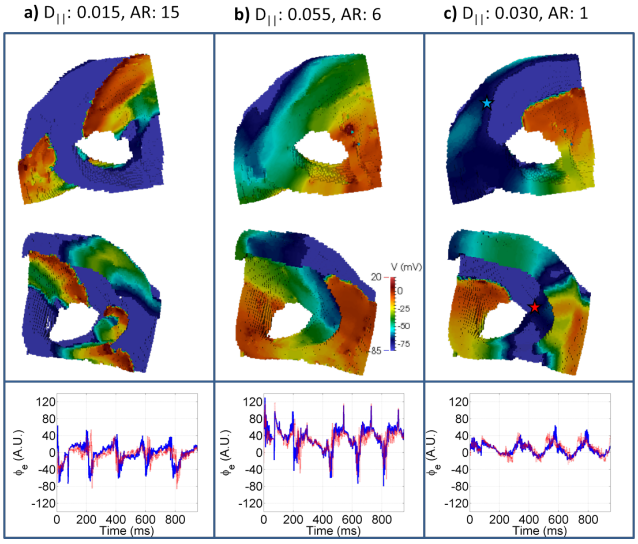

Fig. 4. Re-entry in a segment of the right atrium. Posterior and anterior views of electrical potential maps at t = 750 ms (top row, scale shown in panel b)) and two representative electrode tracings (bottom row) for realistic fiber orientations, with the longitudinal diffusion coefficient ($D_{||}$, in mm^2/ms) and diffusion anisotropy ratio (AR) for each panel shown above it. The position of the electrodes whose traces are displayed is marked by two matching-color stars in panel c).

As in previous studies [10], we found that reentry in 2D tissue did not cause electrogram fractionation per se, but led to a change in the symmetry of the activation peaks. Similarly, in a realistic 3D atrial geometry, the existence of re-entry did not change the degree of fractionation, but only increased the interval during which it occurred, as non-local tissue was continuously excited.

The magnitude of the fractionated signal relative to the local activation peak was found to depend strongly on the degree of intercellular coupling - for low $D_{||}$ values, the local activation becomes more obscured, as its magnitude approaches that of the far-field signal. An increase in the distance between the electrodes and the atrial tissue, which can naturally occur during beating of the heart, will also lead to a decrease in electrogram peaks.

We also found that action potential arrival time estimates based on finding the maximum deflection point in unipolar electrograms [18] became increasingly unreliable when electrograms showed a higher degree of fractionation, which, in our simulations, occurred with a decrease in diffusion coefficient and increasing complexity of local fiber fields. As both these effects become more severe with the progression of AF, errors related to arrival time and detection of breakthrough events [18] are expected to

become more likely, especially when using electrode arrays with low spatial resolution.

Limitations of the study include the use of a monodomain, rather than bidomain model and the assumption that electrodes are small enough to be well approximated by a single point. We have used a cross-field protocol to generate re-entry, but aim in future to use premature stimuli, as we have done in previous studies of re-entry in the pulmonary veins [14], [17] and the whole atria [20]. This will more closely mimic re-entry initiation as performed in animal experiments. Future work will also aim to provide experimental validation to these findings, as well as establish a more quantitative relationship between the degree of fractionation and properties of the tissue, such as AR and $D_{||}$, as proposed recently [21].

In summary, we have found that fractionated electrograms can occur in 2D tissue in the presence of a non-uniform and anisotropic fiber arrangement and in 3D tissue (either isotropic or anisotropic) in the presence of irregular tissue geometry. The presence of one or more re-entry circuits did not qualitatively affect the degree of fractionation of the electrograms. Therefore, electrogram fractionation reflects alterations in the atrial substrate (decrease in intercellular coupling and myofiber organization) required for the sustenance of re-entrant circuits to a greater degree than the existence of abnormal electrical activity in itself. These findings may help explain the variable success rates of clinical ablations procedures where CFAEs are commonly associated with the presence of re-entrant drivers for AF.

V. ACKNOWLEDGMENTS

We acknowledge support from the National Institute for Health Research (NIHR) comprehensive Biomedical Research Centre award to Guy's & St Thomas' NHS Foundation Trust in partnership with King's College London and King's College Hospital NHS Foundation Trust.

REFERENCES

[1] G. Lee, P. Sanders, and J. M. Kalman, "Catheter ablation of atrial arrhythmias: state of the art.," *Lancet*, vol. 380, no. 9852, pp. 1509–19, 2012.

[2] K. Nademanee, J. McKenzie, E. Kosar, M. Schwab, B. Sunsaneewitayakul, T. Vasavakul, C. Khunnawat, and T. Ngarmukos, "A new approach for catheter ablation of atrial fibrillation: mapping of the electrophysiologic substrate," *J. Am. Coll. Cardiol.*, vol. 43, pp. 2044–53, June 2004.

[3] L. Saghy, D. J. Callans, F. Garcia, D. Lin, F. E. Marchlinski, M. Riley, S. Dixit, W. S. Tzou, H. M. Haqqani, R. Pap, S. Kim, and E. P. Gerstenfeld, "Is there a relationship between complex fractionated atrial electrograms recorded during atrial fibrillation and sinus rhythm fractionation?," *Hear. Rhythm*, vol. 9, pp. 181–8, Feb. 2012.

[4] K. T. Konings, J. L. Smeets, O. C. Penn, H. J. Wellens, and M. A. Allessie, "Configuration of Unipolar Atrial Electrograms During Electrically Induced Atrial Fibrillation in Humans," *Circulation*, vol. 95, pp. 1231–1241, Mar. 1997.

[5] A. Verma, R. Mantovan, L. Macle, G. De Martino, J. Chen, C. A. Morillo, P. Novak, V. Calzolari, P. G. Guerra, G. Nair, E. G. Torrecilla, and Y. Khaykin, "Substrate and Trigger Ablation for Reduction of Atrial Fibrillation (STAR AF): a randomized, multicentre, international trial.," *Eur. Heart J.*, vol. 31, pp. 1344–56, June 2010.

[6] J. M. T. de Bakker and F. H. M. Wittkampf, "The pathophysiologic basis of fractionated and complex electrograms and the impact of recording techniques on their detection and interpretation.," *Circ. Arrhythm. Electrophysiol.*, vol. 3, pp. 204–13, Apr. 2010.

[7] M. S. Spach, W. T. Miller, E. Miller-Jones, R. B. Warren, and R. C. Barr, "Extracellular potentials related to intracellular action potentials during impulse conduction in anisotropic canine cardiac muscle," *Circ. Res.*, vol. 45, pp. 188–204, Aug. 1979.

[8] V. Jacquemet and C. S. Henriquez, "Loading effect of fibroblast-myocyte coupling on resting potential, impulse propagation, and repolarization: insights from a microstructure model.," *Am. J. Physiol. Heart Circ. Physiol.*, vol. 294, pp. H2040–52, May 2008.

[9] D. D. Correa de Sa, N. Thompson, J. Stinnett-Donnelly, P. Znojkiewicz, N. Habel, J. G. Müller, J. H. T. Bates, J. S. Buzas, and P. S. Spector, "Electrogram fractionation: the relationship between spatiotemporal variation of tissue excitation and electrode spatial resolution.," *Circ. Arrhythm. Electrophysiol.*, vol. 4, pp. 909–16, Dec. 2011.

[10] V. Jacquemet, N. Virag, Z. Ihara, L. Dang, O. Blanc, S. Zozor, J.-M. Vesin, L. Kappenberger, and C. Henriquez, "Study of Unipolar Electrogram Morphology in a Computer Model of Atrial Fibrillation," *J. Cardiovasc. Electrophysiol.*, vol. 14, pp. S172–S179, Oct. 2003.

[11] R. J. Ramirez, S. Nattel, and M. Courtemanche, "Mathematical analysis of canine atrial action potentials : rate , regional factors , and electrical remodeling," *Am J Physiol Hear. Circ Physiol*, vol. 279, pp. 1522–1539, Oct. 2000.

[12] O. V. Aslanidi, T. D. Butters, C. X. Ren, G. Ryecroft, and H. Zhang, "Electrophysiological models for the heterogeneous canine atria: computational platform for studying rapid atrial arrhythmias.," *Conf. Proc. IEEE Eng. Med. Biol. Soc.*, vol. 2011, pp. 1693–6, Jan. 2011.

[13] U. Schotten, S. Verheule, P. Kirchhof, and A. Goette, "Pathophysiological mechanisms of atrial fibrillation: a translational appraisal.," *Physiol. Rev.*, vol. 91, pp. 265–325, Jan. 2011.

[14] O. V. Aslanidi, T. Nikolaidou, J. Zhao, B. H. Smaill, S. H. Gilbert, A. V. Holden, T. Lowe, P. J. Withers, R. S. Stephenson, J. C. Jarvis, J. C. Hancox, M. R. Boyett, and H. Zhang, "Application of micro-computed tomography with iodine staining to cardiac imaging, segmentation, and computational model development.," *IEEE T Med Imaging*, vol. 32, no. 1, pp. 8–17, 2013.

[15] M. Varela, J. Zhao, and O. V. Aslanidi, "Determination of Atrial Myofibre Orientation Using Structure Tensor Analysis for Biophysical Modelling," in *Funct. Imaging Model. Hear. SE - 50* (S. Ourselin, D. Rueckert, and N. Smith, eds.), vol. 7945 of *Lecture Notes in Computer Science*, pp. 425–432, Springer Berlin Heidelberg, 2013.

[16] O. V. Aslanidi, M. A. Colman, M. Varela, J. Zhao, B. H. Smaill, J. C. Hancox, M. R. Boyett, and H. Zhang, "Heterogeneous and anisotropic integrative model of pulmonary veins: computational study of arrhythmogenic substrate for atrial fibrillation," *Interface Focus*, p. doi: 10.1098/rsfs.2012.0069, 2013.

[17] M. A. Colman, M. Varela, J. C. Hancox, H. Zhang, and O. V. Aslanidi, "Evolution and pharmacological modulation of the arrhythmogenic wave dynamics in canine pulmonary vein model.," *Europace*, vol. 16, pp. 416–23, Mar. 2014.

[18] J. Eckstein, S. Zeemering, D. Linz, B. Maesen, S. Verheule, A. van Hunnik, H. Crijns, M. A. Allessie, and U. Schotten, "Transmural conduction is the predominant mechanism of breakthrough during atrial fibrillation: evidence from simultaneous endo-epicardial high-density activation mapping.," *Circ. Arrhythm. Electrophysiol.*, vol. 6, pp. 334–41, Apr. 2013.

[19] W. G. Stevenson and K. Soejima, "Recording techniques for clinical electrophysiology.," *J. Cardiovasc. Electrophysiol.*, vol. 16, pp. 1017–22, Sept. 2005.

[20] M. A. Colman, O. V. Aslanidi, S. Kharche, M. R. Boyett, C. J. Garratt, J. C. Hancox, and H. Zhang, "Pro-arrhythmogenic effects of atrial fibrillation-induced electrical remodelling: insights from the three-dimensional virtual human atria.," *J. Physiol.*, vol. 591, pp. 4249–72, Sept. 2013.

[21] F. O. Campos, T. Wiener, A. J. Prassl, R. W. dos Santos, D. Sanchez-Quintana, H. Ahammer, G. Plank, and E. Hofer, "Electroanatomical characterization of atrial microfibrosis in a histologically detailed computer model.," *IEEE Trans. Biomed. Eng.*, vol. 60, pp. 2339–49, Aug. 2013.